Radio Science, Volume 33, Number 2, Pages 369–392, March–April 1998

Remotely sensing cloud properties from microwave radiometric observations by using a modeled cloud database

Giovanni d'Auria, F. S. Marzano,[1] N. Pierdicca and R. Pinna Nossai
Dipartimento di Ingegneria Elettronica, Università "La Sapienza" di Roma, Rome, Italy

Patrizia Basili
Istituto di Elettronica, Università di Perugia, Perugia, Italy

Piero Ciotti
Dipartimento di Ingegneria Elettrica, Università dell'Aquila, L'Aquila, Italy

Abstract. As a first step for remote sensing cloud properties, a database of cloud genera has been established. This is derived from a microphysical model, and it considers the statistical profiles of four hydrometeor species for each cloud genus. From this database the corresponding radiative database is obtained making use of a radiative transfer model, so for each cloud genus the simulated microwave response at the special sensor microwave imager channels is found. The cloud and radiative databases allow the retrieval of the genera of the cloud and other relevant properties from satellite observations. An automatic cloud genus classifier has also been implemented. Several tests have been carried out, and the results are presented.

1. Introduction

A thorough description of cloud properties is essentially based on the knowledge of the vertical profiles of the densities of the hydrometeors present in the cloud itself. At least four hydrometeors are generally accepted as sufficient for such a description: raindrops, cloud water droplets, graupel particles, and ice crystals [*Smith et al.*, 1992]. The possibility of remotely sensing these properties by passive sensors relies, at present, on using visible, infrared, or microwave channels. Visible (VIS) and infrared (IR) sensors cannot see inside the clouds, and information on their properties can only be gained indirectly by using the albedo and the temperature of the cloud top, which these sensors are able to give [*Desbois et al.*, 1982; *Garand*, 1988]. However, it is still necessary to have a database of clouds at least grouped according to their top albedo and temperature or whatever we have. The multichannel microwave observation of the brightness temperature (T_B) of clouds has been recognized to be promising because these sensors respond to many more details of the cloud properties [*Mugnai et al.*, 1993; *Kummerow and Giglio*, 1994]. However, again we need a database of almost all kinds describing their hydrometeor profiles and the corresponding brightness temperatures they produce. Few cases of hydrometeor profile retrieving are found in the literature [*Basili et al.*, 1995 ; *Evans et al.*, 1995; *Kummerow et al.*, 1996; *Pierdicca et al.*, 1996]. In most cases, attention is mainly focused on retrieving precipitation intensity or areas of probable precipitation, and the algorithms used are often empirical [*Ferraro et al.*, 1994].

For remotely sensing cloud properties it is indeed necessary to establish a reliable database of clouds in order to find their microwave signature, that is, their radiative response. Since clouds can exist in a variety of hydrometeor profiles, it is worthwhile to group them in a suitable way so that all possible realizations of a single cloud type are statistically defined. Correspondingly, by using a radiative transfer model, the statistical database of brightness temperatures which can be observed by a satellite-based radiometer, for that type of cloud, turn

[1]Now at Dipartimento di Ingegneria Elettrica, Università dell'Aquila, L'Aquila, Italy.

Paper number 97RS02397.
0048-6604/98/97RS-02397$11.00

out to be defined. However, it is well known that few experimental data exist in literature for setting up a reliable database [*Pruppacher and Klett*, 1978; *Bogush*, 1989], so that very often one has to rely on cloud models strictly based on the microphysics of cloud events. These models often refer to particular types of clouds resulting from a specific meteorological event, but if it is possible to follow its space-time evolution, samples of more varieties of clouds become included. As a starting point for producing a cloud database, a microphysical model can be adopted to describe the evolving and decaying phases of specific precipitating events. Modifications are therefore needed for generating a more general database comprehensive of almost all kinds of clouds and for different climatic areas. At this point it is necessary to choose how to group and define the diverse kinds of clouds. This is one of the major problems because the choice determines the possibility of recognizing the type of cloud from radiometric measurements and also validating the results. A clustering procedure has been adopted elsewhere [*Pierdicca et al.*, 1996], which is able to subdivide the entire database into a given number of classes of more or less different microphysical characteristics, recognizable as different kinds of clouds. This attribution is impaired, however, by the fact that different kinds of clouds sometimes merge into the same class and that some cloud events are scarcely represented in a given class.

In this paper we have assumed, as a microphysical model, the University of Wisconsin Nonhydrostatic Modeling System (UW-NMS) described by *Tripoli* [1992], and we have followed a procedure, different from the clustering technique, for grouping the database provided by the model itself. Classes are formed directly by sorting out the realizations of clouds that comply with requirements of the standard meteorological definition. This is based on the International Cloud Atlas [*World Meteorological Organization*, 1971] and considers four types of clouds: cumulus, stratus, cirrus, and nimbus. Further specifications with composite names (genera) are also used: altocumulus, altostratus, cumulonimbus, and nimbostratus, but the indication of the species is only considered in a few cases. The choice of this classification is appealing because in many cases the "truth" may be ascertained by simple visual inspection from the ground sometimes provided by meteorological centers. All profiles of the set of data furnished by the microphysical model have been examined, and by considering the content of the hydrometeors at various altitudes, they have been assigned to a specific genus of cloud. This selection has been made by taking into account the physics of each genus as derived from the meteorological definition of its development process. Since the assumed model and its corresponding database refer to a specific evolving storm, not all the cloud genera are found (or some of them are found only in a number of realizations not statistically significant). Therefore some modifications have been introduced. The number of realizations for each genus has been increased by means of a Gaussian random generation which, however, preserves the original correlation matrix of the density of the hydrometeors at the various levels (thus ensuring the same microphysical nature as the assumed cloud model) and also by modifying in some cases the average value (or the variance or both) of a given class (as in the case of cloud stratus, for instance).

For the obtained database of each cloud genus a corresponding brightness temperature database is produced making use of a plane-parallel radiative transfer model, implemented for the seven channels of the special sensor microwave imager (SSM/I). The simulation of the satellite observations includes specific kinds of background. The choice of a horizontally homogeneous radiative transfer model is a limiting factor. On the other hand, the introduction of a horizontally limited extension of cloud would impose a number of geometrical parameters difficult to cope with. In some cases this limitation is overcome by using a filling factor relative to the field of view of the radiometer antenna. Such a filling factor may be related to the genus of cloud we are observing, and a rough estimation could be given. The texture pattern of some kinds of clouds can be statistically estimated in some cases, but the problem of the knowledge of the background arises. This requires an observation long enough to contain samples of clear-sky conditions. The creation of a microphysical consistent cloud database and the corresponding radiative database of simulated brightness temperatures is only the starting point. Through validation tests and experimental results, modifications of the genus database may well occur subsequently.

Direct tests for validating the results (profiles or integrated values of hydrometeors) are obviously difficult to make, but indirect comparisons can make use of other kinds of observations and analyses to establish how good the results are. These are (1) visual inspection of the sky from ground; (2) rain gauge network measurements; (3) status and evolution of meteorological conditions described by meteorological maps (front passages and so on); (4) cloud climatology in a given area; (5) ra-

dar maps; (6) microwave radiometric measurements from ground; and (7) data from satellites in VIS and IR channels. Some examples of these comparisons are reported. Finally, an automatic classifier, derived from the obtained cloud database, has been implemented. This make it possible to find the most probable genus of cloud given a set of microwave radiometric measurements from the satellite.

2. Generation of a Cloud Database Based on Genus Classification

The input for the generation of the cloud database is the UW-NMS microphysical model [*Tripoli*, 1992]. This model is three dimensional and time dependent and considers four different kinds of hydrometeors: precipitating liquid water (raindrops), nonprecipitating liquid water (cloud droplets), precipitating ice (graupel particles), and nonprecipitating ice (ice crystals and aggregates). Statistical relationships exist among the contents of these hydrometeor species which are related to microphysics of the space-time evolution process of the cloud [*Basili et al.*, 1995]. The model gives a 4-hour simulation of an intense summer hailstorm that occurred near Eldridge, Alabama. The hydrometeor profiles were sampled every 1 min throughout the course of the simulation at a horizontal resolution of 1 km and a vertical resolution of about 0.5 km (42 altitude levels).

Although not strictly necessary, some simplifications in the use of this model were introduced [*Smith et al.*, 1992]. The hydrometeor contents were expressed by their equivalent water content (EWC), and the profiles were horizontally averaged within 10-km square boxes. Therefore 774 cloud structures are obtained consisting of four EWC profiles for each hydrometeor, three profiles of meteorological parameters (pressure, temperature, and specific humidity), and the value of the surface rain rate. To proceed to the generation of a new database, we have intended these 774 profiles to be realizations of the random process generating the cloud structure. In other words, we have supposed that the cloud structure generated by the model as a function of space and time can represent different statistical realizations of a cloud. By examining each realization of the vertical profiles and bearing in mind its evolution, we can get essential information on the structure of the kind of cloud that each profile represents.

It is well known that the subdivision of clouds into different genera and species, according to the International Cloud Atlas, has a historical origin. This classification is founded on the visual aspect of the cloud seen from the ground, that is, its vertical and horizontal extent, its shape, its contours, its texture, its transparency (or opacity), and the effects it produces (rain, lightning, etc.). However, by putting together these visual observations with the physics of the formation of clouds (essentially based on the atmosphere's stability, vertical air motion, and changing of water phases), a bulk of information on the hydrometeor contents inside the clouds has been obtained. In addition, other information can be derived from radar observations and in situ measurements. All this store of information makes it possible to ascribe each profile of the original microphysical model to a certain genus of cloud and sometimes even specify the species or particular attribute of the cloud. The guidelines for this recognition are based on some basic points: the vertical extension (top and bottom altitudes), the concentration of each hydrometeor species at the various altitudes, the intensity of rain (if any), and the stage of the evolution in which a given profile stands.

Table 1 summarizes the main characteristics of each genus for which the recognition was feasible and the database was produced. Besides the genus symbol and the bottom and top altitudes, the maxima of columnar EWC (CEWC) and surface rainfall rate (RR) are shown. Note that stratus, nimbostratus, altocumulus, and cirrus genera were not met in a sufficient number within UW-NMS and that we have had to supply information regarding the mean value of the hydrometeor content and other statistical parameters. The remaining cloud genera, that is, stratocumulus, cirrostratus, and cirrocumulus, have been disregarded during the classification due to their close similarity in the vertical distribution of hydrometeors with stratus and cirrus.

Some common characteristics of the diverse cloud genera are worth noting in Table 1. Clouds could further be grouped in different ways, for instance, according to their top and bottom altitudes, the vertical extension, the rain rate they produce, or other ways. As will be explained later, these considerations will be useful when trying to verify the quality of a classification based on a genus database or, in other words, if the database assigned to a certain cloud genus really represents satisfactorily that cloud. Indeed, other sensors like those at IR and VIS band or in situ meteorological measurements, like rain gauge measurements themselves, can identify a group of cloud genera and not a single one. Therefore, by using diverse observations, it becomes possible to attempt a comparison with the truth by intersecting identified groups of cloud genera. For instance,

Table 1. Main Characteristics of the Simulated Cloud Genera

Cloud Genus and Species	Abbreviation	Bottom Altitude, km	Top Altitude, km	Maximum Cloud CEWC, kg/m^2	Maximum Rain CEWC, kg/m^2	Maximum Graupel CEWC, kg/m^2	Maximum Ice CEWC, kg/m^2	Maximum Surface Rain Rate, mm/h
Cumulus mediocris	Cu med	1.5-2	8.5	1.0	0	0	0.5	0
Cumulus congestus	Cu con	0-1	14	1.8	5.6	2.4	2.0	36
Cumulonimbus	Cb	0.-1	16	1.8	11.1	8.6	4.4	114
Cumulonimbus with incus	Cb incus	0.4-1	16	1.4	6.5	6.5	4.6	75
Stratus	St	0.5	2.5	0.5	0.2	0	0	2
Nimbostratus	Ns	0.1-1	9.5	1.8	1.8	0.4	0.2	15
Altostratus	As	1.5-2	7	0.4	0.5	0	0.1	3
Altocumulus	Ac	2-3	4	0.2	0	0	0	0
Cirrus	Ci	6-8	11.5	0	0	0	1.1	0

CEWC, columnar equivalent water content.

clouds producing heavy rain are mainly limited to three genera: some species of cumuli, cumulonimbi, and nimbostrati, which, however, present different properties in their evolution, altitudes, and so on. Consequently, these clouds are seen as belonging to different groups by sensors like IR and VIS band radiometers.

Once the subdivision into classes of genera is performed, we can calculate the statistical parameters of each class. The profile is described by a vector $\mathbf{g}$ of dimension D, given by the four hydrometeor EWCs multiplied by the number of samples along the altitude. We can estimate the covariance matrix $\mathbf{C}g$ of the class through the following equation:

$$\mathbf{C}_g = (N-1)^{-1} \sum_{i=1,N} \Delta\mathbf{g}_i \Delta\mathbf{g}_i^T \quad (1)$$

where N is the number of available profiles belonging to the class and $\Delta\mathbf{g}$ is the difference vector between $\mathbf{g}$ and its mean vector $\mathbf{m}$.

The covariance matrix $\mathbf{C}g$ and the mean vector $\mathbf{m}$ represent quantitative characteristics of the given class of cloud, and they resume the statistical properties of that cloud in agreement with microphysical laws which have produced it. We can use these quantities to enlarge the statistical database. Indeed, we have increased to 4500 the number of realizations of all the cloud genera. This is particularly necessary for certain classes which contain a small number of elements. By assuming a Gaussian distribution defined by matrix $\mathbf{C}g$ and vector $\mathbf{m}$, it is possible to perform a pseudo-random generation of realizations, which will be Gaussian distributed but limited only to positive values of the parameters [*Pierdicca et al.*, 1996].

For an easier handling of each database, further simplifications have been introduced. The vertical structure constituted by 41 layers (the original sampling resolution) has been reduced to seven layers by a staircase approximation. This layer reduction has been performed for each hydrometeor EWC profile, and an average EWC value has been attributed to each layer. Each individual structure is therefore identified by at most 7x4 values of EWC plus the surface rain rate, for a total of 29 variables. However, not all the layers of a given class contain every kind of hydrometeor, and this reduces considerably the number of hydrometeor parameters needed to describe a cloud genus. Moreover, in some cases in order to render more visible the peculiarity of a class, the columnar EWCs of a hydrometeor are also given.

During the generation we have randomly varied the cloud genus levels around the levels of the mean profiles $\mathbf{m}$, taking care to eliminate realizations producing layers of zero (or even negative) thickness. Moreover, we have supposed the meteorological parameters to be variable around the mean meteorological profile as a consequence of random variations of the surface temperature (T_s) and specific humidity (q_s). In this way we have generated four cloud databases for spring, summer, autumn,

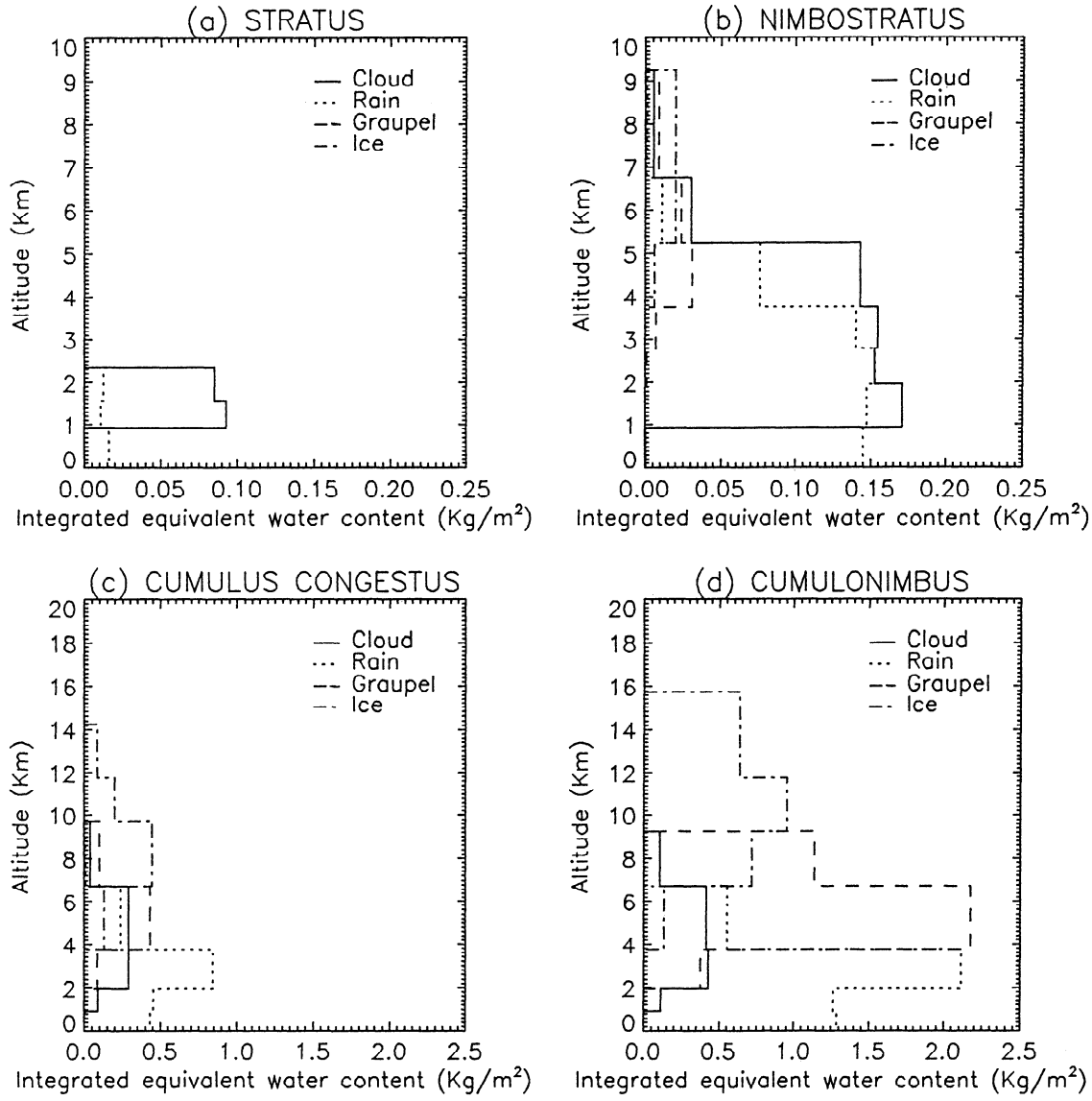

Figure 1. Mean vertical profiles of simulated cloud genera: (a) stratus; (b) nimbostratus; (c) cumulus congestus; and (d) cumulonimbus.

and winter conditions. For example, in the summer case we have chosen the mean surface temperature T_s=298 K and mean surface specific humidity q_s=10 g/kg, while in the winter case T_s=283 K and q_s=5 g/kg assuming the vertical gradients and scales of the standard midlatitude atmosphere. However, the meteorological profiles can be adapted to the climatic period and location under analysis. The seasonal cloud databases are substantially different from each other. This structural difference arises from the fact that the change of the meteorological profiles has imposed the modification of the vertical distribution of the hydrometeor contents in order to preserve a physical consistency of the cloud structure. For example, by decreasing the negative thermal vertical gradient, the zero thermal altitude and the cloud top height are changed, thus eliminating the rain layer above the new zero thermal height and increasing the thickness of ice crystal and aggregate layers.

Figure 1 shows representative profiles of EWCs integrated within each layer of the four hydrometeors for

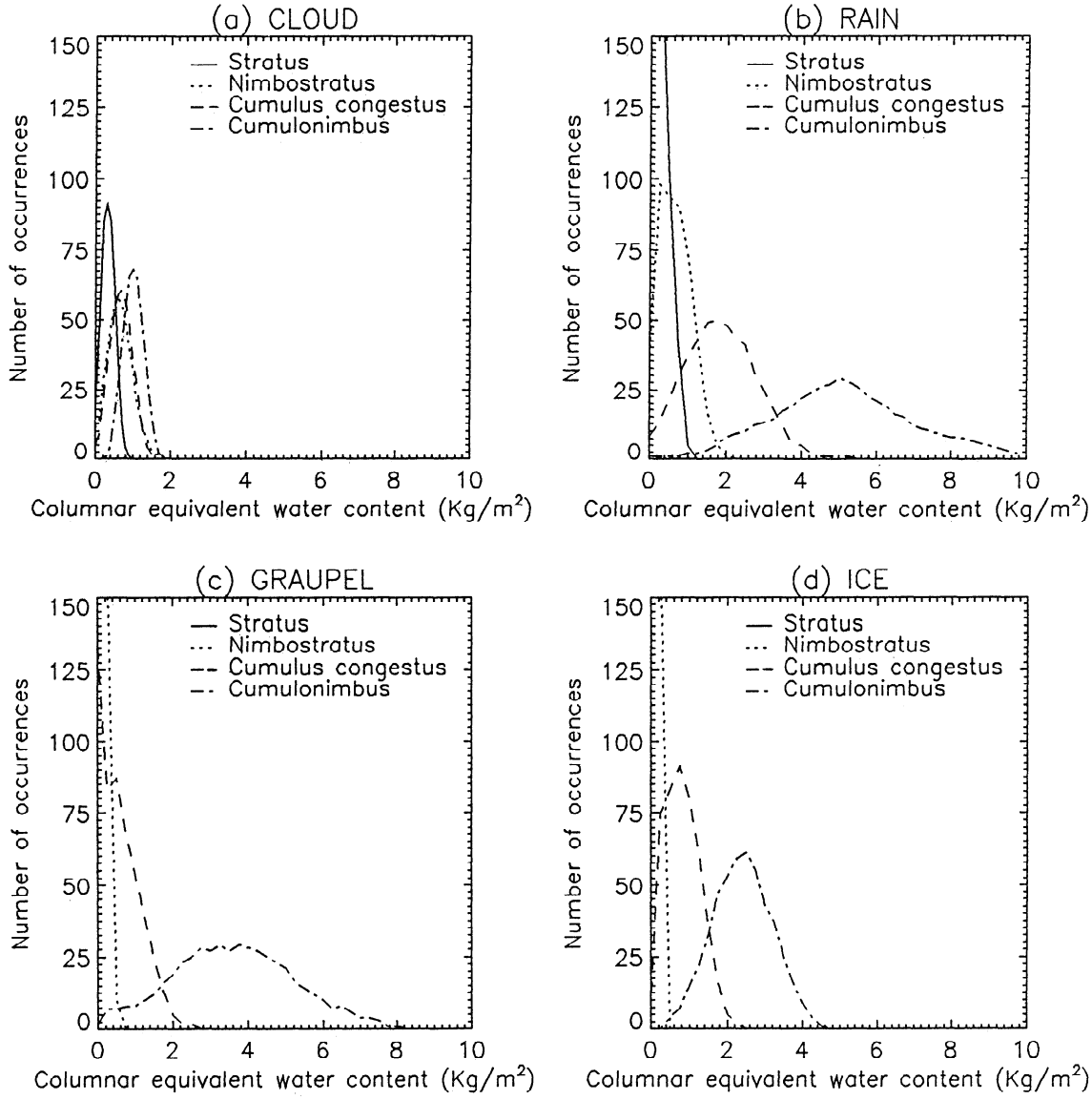

Figure 2. Histograms of columnar equivalent water content (EWCs) of each hydrometeor for the same cloud genera as in Figure 1: (a) cloud droplets; (b) rain drops; (c) graupel particles; and (d) ice crystals and aggregates.

some of the considered cloud genera, that is, stratus, nimbostratus, cumulus congestus, and cumulonimbus, supposing summer conditions. It is noted that when reducing the vertical resolution to seven layers by staircase approximation, mean depths and heights of the layers are different for each cloud genus. As expected, stratiform clouds show little or no graupel and ice layers, while the cumuliform ones have a more complicated vertical structure characterized by a strong presence of both liquid and frozen water.

Another view of the database properties of each cloud genus is illustrated in Figure 2, where histograms of columnar values of hydrometeor EWC over the entire realizations of the cloud genus are depicted for the same cloud genera of Figure 1. Note that cumulonimbi show mean values of CEWC of rain and graupel of about 5

and 4 kg/m^2, respectively, which are much higher than those of cumuli congesti and nimbostrati.

3. Radiative Model for Simulating Satellite Radiometric Observations

For producing simulated brightness temperatures from the cloud database, a radiative transfer model is assumed, with some simplifying assumptions. The correctness of these assumptions has to be subjected to long lasting verifications, and there is no doubt that further improvements are liable to come. The assumptions mainly regard the formulation of the radiative transfer equation (RTE) and its numerical solution and the absorption and scattering properties of the hydrometeors themselves. These depend on the hydrometeor shape, dielectric properties, and size distributions.

The cloudy atmosphere has been supposed to be horizontally homogeneous and azimuthally symmetric. No polarization effects are considered so that the RTE has the following form:

$$\mu \frac{dT_B(\mu,\tau)}{d\tau} = -T_B(\mu,\tau)+J(\mu,\tau) \qquad (2)$$

where T_B is the unpolarized brightness temperature, μ is the cosine of the zenithal angle, τ is the zenithal optical thickness, and $J(\mu,\tau)$ is the source function defined as

$$\begin{aligned} J(\mu,\tau) &= (1-w)T(\tau)+\frac{w}{2}\int_{-1}^{+1} p(\mu,\mu')T_B(\mu',\tau)d\mu' \\ &= J_e(\mu,\tau)+J_s(\mu,\tau) \end{aligned} \qquad (3)$$

In equation (3), w represents the albedo, T is the physical temperature of the medium, and p is the phase function, while the source function J has been decomposed into emission (J_e) and multiple scattering (J_s) components.

Since the solution of equation (2) can be written in terms of an integration from the Earth's surface (z=0) to the satellite height (z=∞), it is useful to appreciate the radiative contribution (both in emission and scattering) to the observed brightness temperature from the satellite coming from each cloud layer [*Wu and Weinman*, 1984; *Mugnai et al.*, 1993]. To this end, we introduce a contribution function W, defined as follows:

$$W(\mu,z) = k_e(z)\frac{J(\mu,z)}{\mu}e^{-\frac{\tau(z,\infty)}{\mu}} = W_e(\mu,z)+W_s(\mu,z) \qquad (4)$$

where k_e is the extinction coefficient and $\tau(z,\infty)$ indicates the optical thickness between the altitude z and satellite height.

The solution of RTE has been carried out numerically following the Eddington approximation, specifying the top and bottom boundary conditions and the continuity conditions at the layer interfaces [*Wu and Weinman*, 1984; *Kummerow*, 1993]. For the Earth's surface conditions, both land and sea surfaces have been considered. For the land surface we have assumed a Lambertian model with emissivity given by a regressive relationship involving the ground humidity [*Mugnai and Smith*, 1988]. For the sea surface the water dielectric constant has been parameterized to salinity and temperature [*Stogryn*, 1971]. We have computed polarized V and H upwelling brightness temperatures due to the corresponding V and H components of specular-surface emissivity due to a calm sea. Note that in the latter case we have disregarded the effects of atmospheric depolarizations. We have also computed the unpolarized radiometric response for a rough sea surface by cosine-averaging the vertical (V) and horizontal (H) emissivities derived from Fresnel's coefficients [*Mugnai and Smith*, 1988]. In this case the values of surface emissivity range from 0.42 (at 19 GHz) to 0.56 (at 85 GHz) over the sea and from 0.81 (at 19 GHz) to 0.85 (at 85 GHz) over land. According to the Eddington approximation, the phase function has been assumed as an expansion of Legendre polynomials but limited to the first order. All the hydrometeors have been assumed to be spherical, thus using the Mie formulation to compute asymmetry factors and extinction coefficients. Even though the sphericity assumption is not strictly proper, especially for ice particles, the average phase function of a randomly oriented ensemble of nonspherical particles tends, in general, to approach that of a polydispersion of equal-volume spheres [*Mugnai and Wiscombe*, 1980]. The gaseous absorption has been calculated by means of the Liebe model [*Liebe*, 1985].

The refractive index of each hydrometeor has been calculated by means of the Ray approximation of Debye's formula [*Ray*, 1972]. Cloud droplets and raindrops are considered homogeneous inside so that the dielectric properties are mainly related to their physical temperature. On the contrary, graupel particles, ice crystals, and aggregates have a more complex structure. In particular, graupel particles are derived from ice crystals of different shapes on which, by a riming process, a coat of spongy frozen water is formed. However, graupel parti-

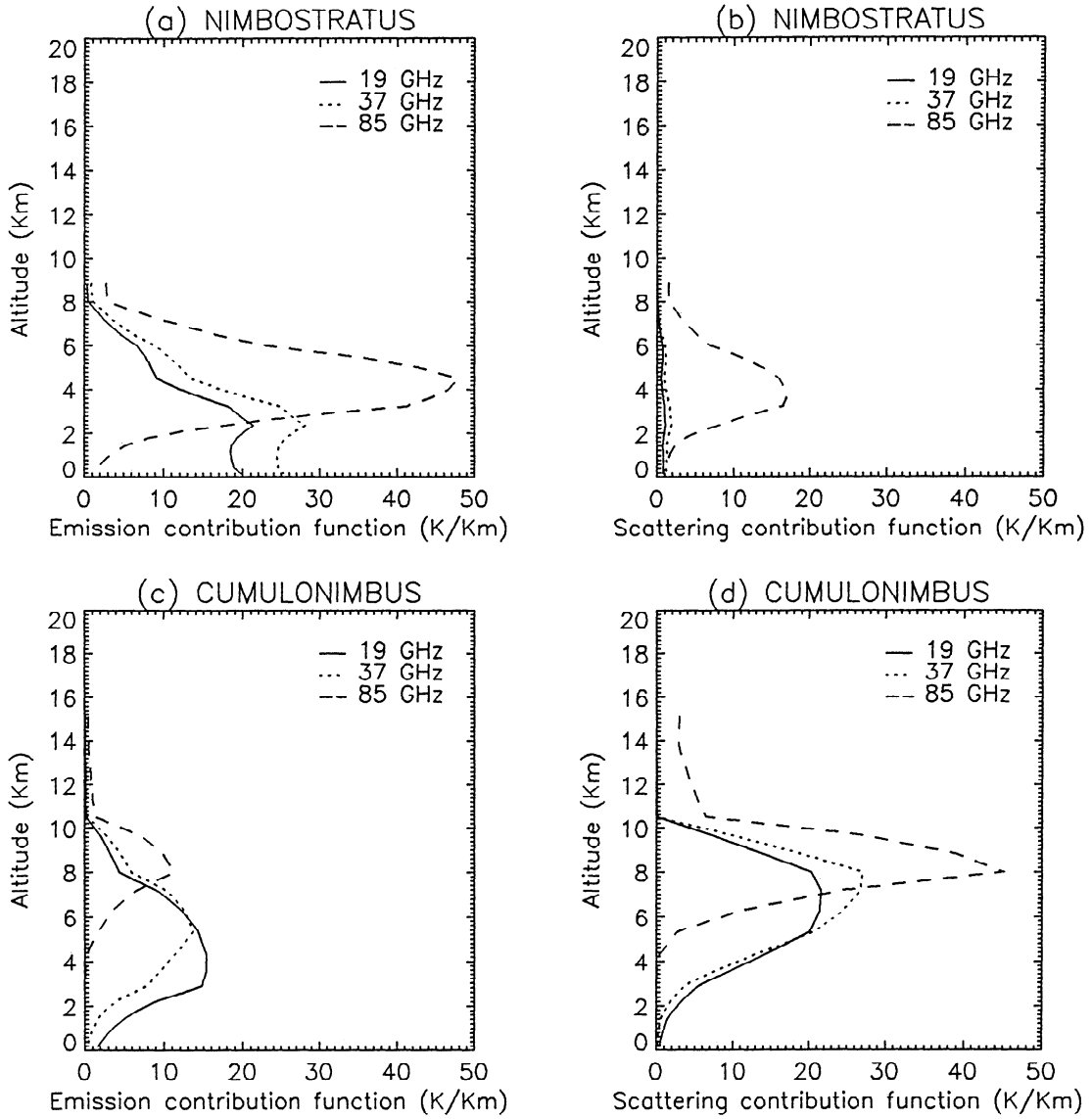

Figure 3. Vertical profiles of emission (Figures 3a and 3c) and scattering (Figures 3b and 3d) contribution functions for nimbostratus (Figures 3a and 3b) and cumulonimbus (Figures 3c and 3d).

cles exist in different stages of formation, running from ice crystals lightly grown by riming to the extreme case of hailstones. The density of these particles varies from 0.6 g/cm^3 for graupel to 0.1-0.2 g/cm^3 for ice crystals and aggregates with air inclusions, modeled by a second-order Maxwell-Garnett approximation [*Bohren and Huffman*, 1983]. As the graupel particles progressively fall and reach the zero thermal altitude or lower, a melting process starts, and a model with a liquid water coat of increasing thickness has been assumed (from 5% around the zero thermal altitude up to 100% when the particles become raindrops).

Besides the importance of the structure and dielectric properties of particles on determining the single-scattering parameters, their size distribution (SD) also plays a major role. In fact, the particle properties must be averaged over the size distribution, and the results of the radiative simulation may be fairly dependent on the assumed distribution. The choice of the size distribution for each hydrometeor has been made from what can be

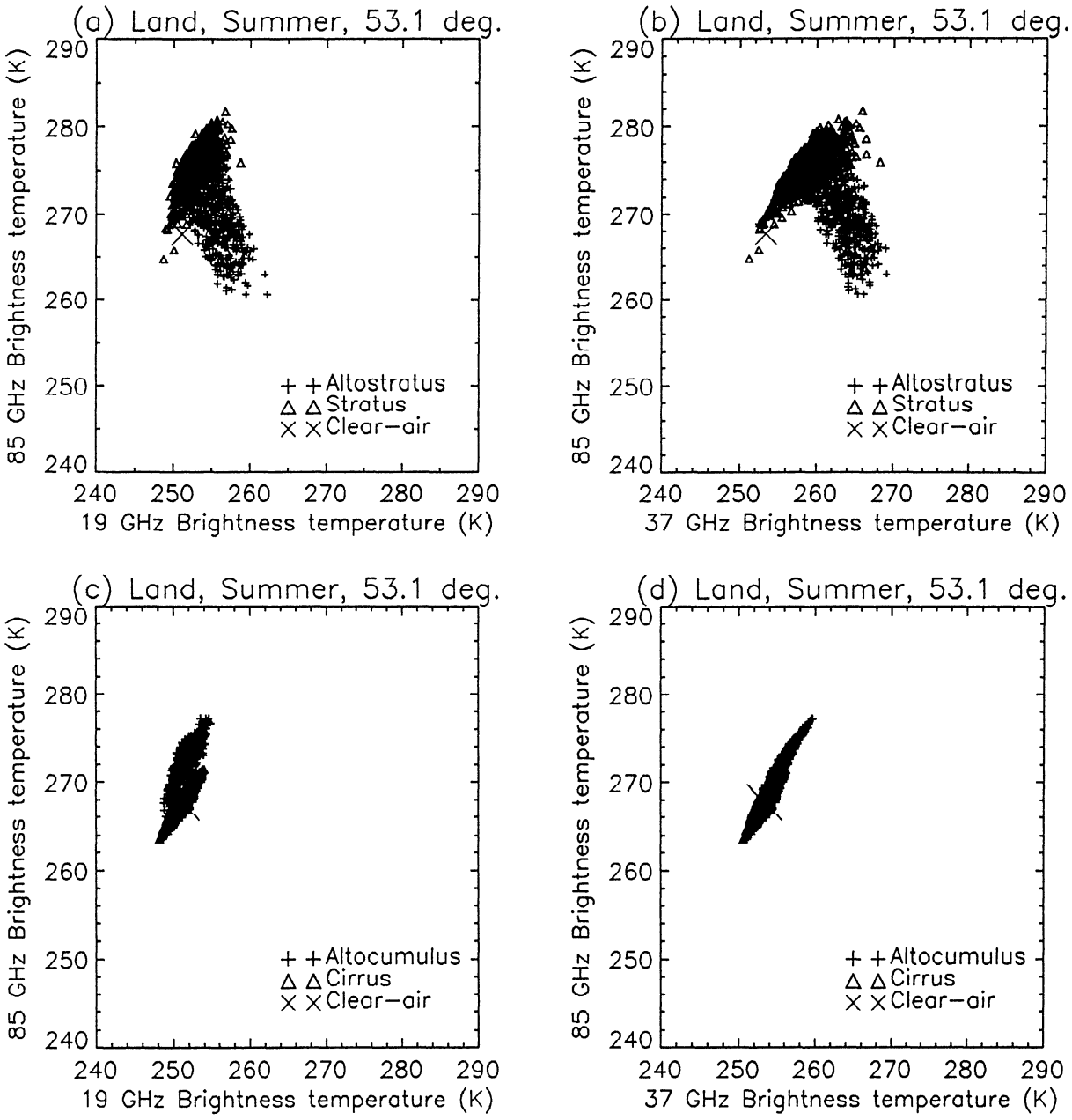

Figure 4. Scatterplots of simulated 85-GHz T_B against 19-GHz T_B (Figures 4a and 4c) and 37-GHz T_B (Figures 4b and 4d) for altostratus and stratus (Figures 4a and 4b) and for altocumulus and cirrus (Figures 4c and 4d) observed at 53.1° off-nadir angle over land during summer. As a reference, T_B values relative to the mean meteorological profiles in clear-air conditions are reported.

found in the literature, but various attempts have been made to match as well as possible the simulated results with measurements from the SSM/I satellite. In general, we have chosen a negative-exponential form of size distribution with the exponent (slope) related to surface rain rate and the total concentration of particles (intercept) derived from the hydrometeor EWC within each layer [*Pruppacher and Klett*, 1978]. Namely, for raindrops we have chosen the well-known Marshall-Palmer SD with radius ranging from 0.1 to 3 mm. Cloud drop-

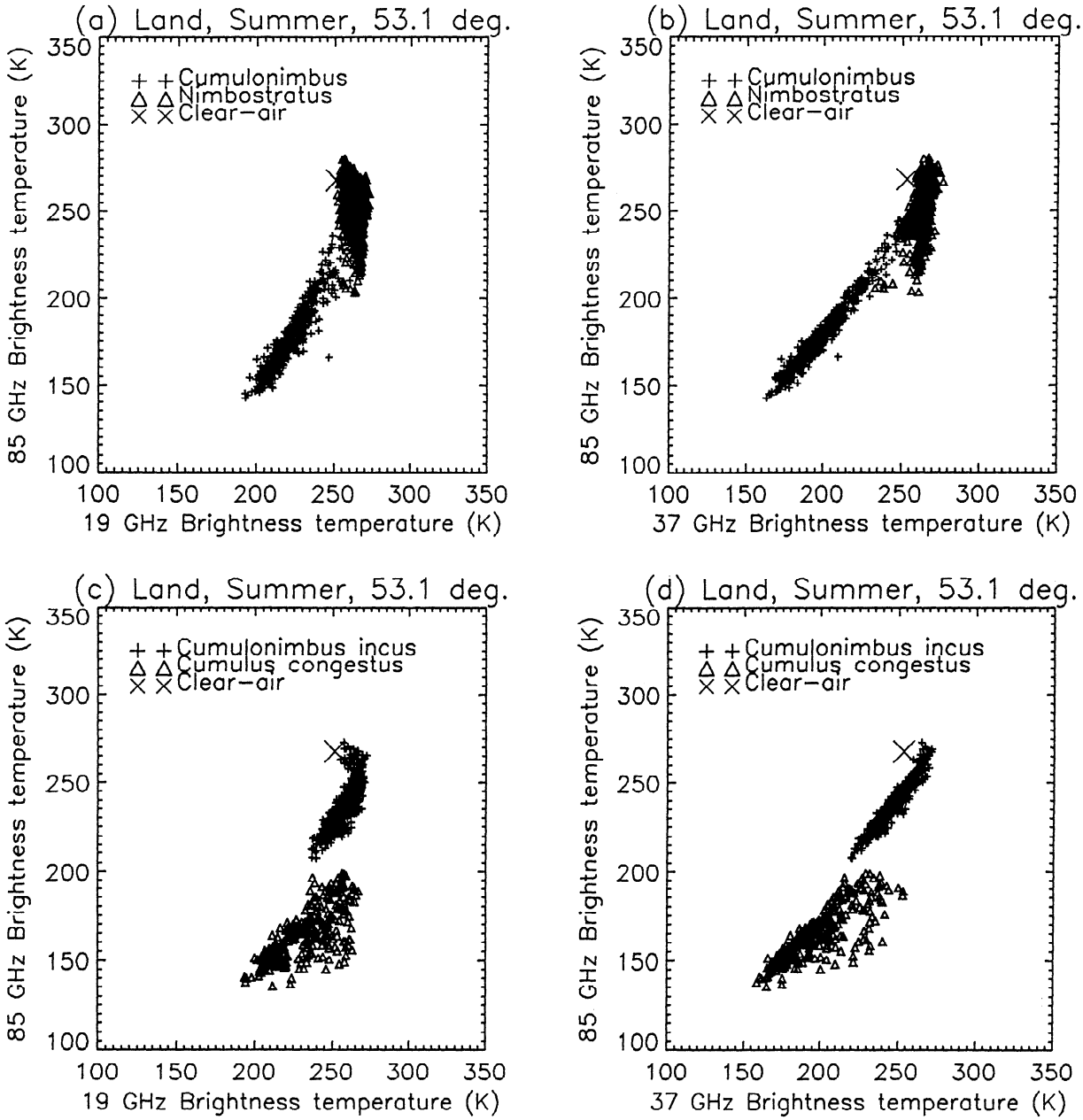

Figure 5. Scatterplots of simulated 85-GHz T_B against 19-GHz T_B (Figures 5a and 5c) and 37-GHz T_B (Figures 5b and 5d) for cumulonimbus and nimbostratus (Figures 5a and 5b) and for cumulonimbus incus and cumulus congestus (Figures 5c and 5d) observed at 53.1° off-nadir angle over land during summer. As a reference, T_B values relative to the mean meteorological profiles in clear-air conditions are reported.

lets have been supposed to be distributed according to a modified Gamma SD ranging from 0.001 to 0.01 mm, respectively. For graupel particles we have chosen the Sekhon-Srivastava SD form [*Sekhon and Srivastava*, 1970] with minimum and maximum radius equal to 0.1 and 5 mm, respectively, while for ice crystals and aggregates we have used the Gunn-Marshall SD with sizes between 0.1 and 10 mm [*Pruppacher and Klett*, 1978].

To gain a physical insight into contributions of brightness temperature reaching the satellite, we report

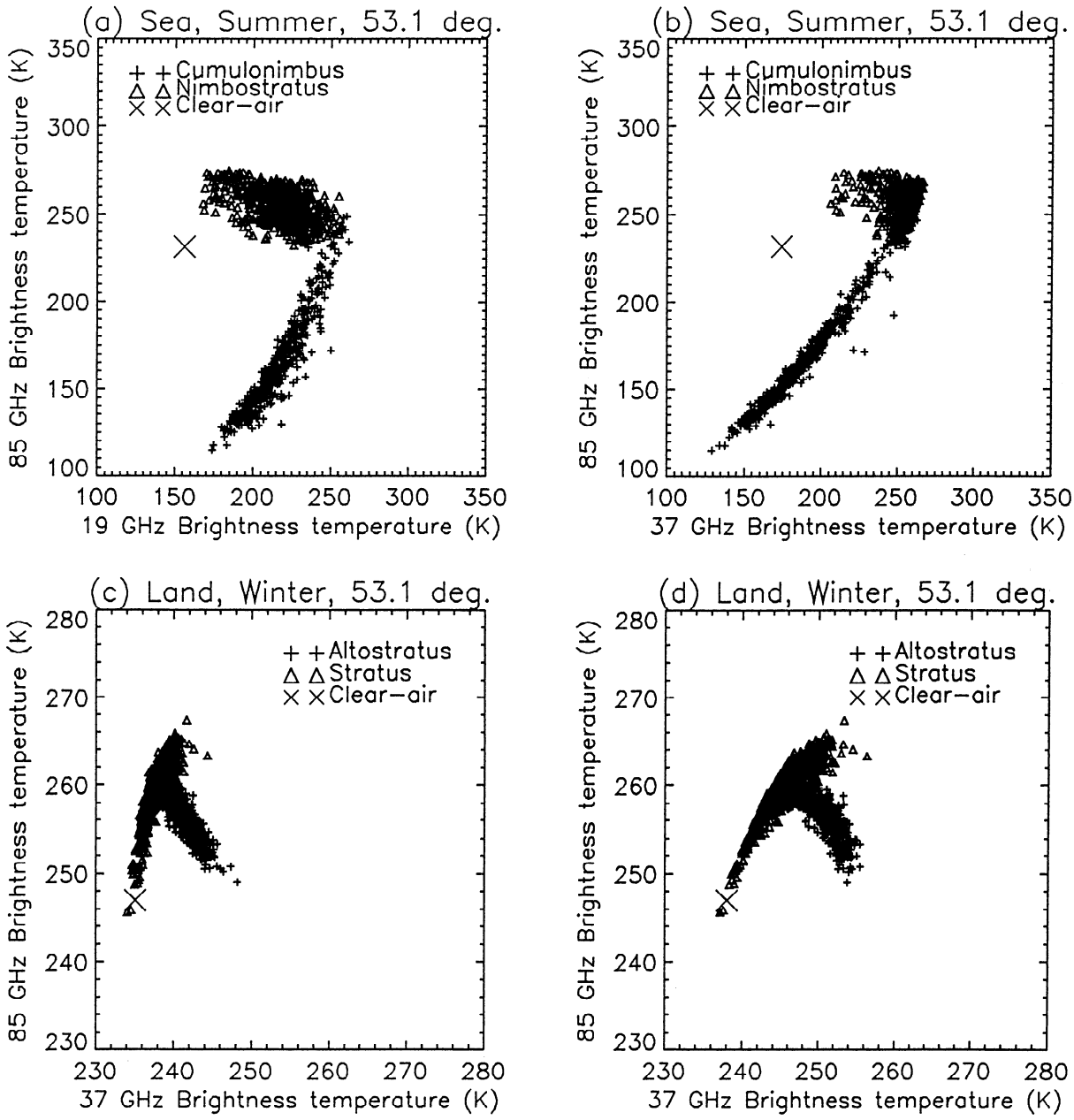

Figure 6. Scatterplots of simulated 85-GHz T_B against 19-GHz T_B (Figures 6a and 6c) and 37-GHz T_B (Figures 6b and 6d) for cumulonimbus and nimbostratus over sea during summer (Figures 6a and 6b) and for altostratus and stratus over land during winter (Figures 6c and 6d) observed at 53.1° off-nadir angle. As a reference, T_B values relative to the mean meteorological profiles in clear-air conditions are reported.

in Figure 3 the vertical profile of the contribution functions W_e and W_s at 19, 37, and 85 GHz for the cumulonimbus (Figures 3a and 3b) and nimbostratus (Figures 3c and 3d) cloud structures, shown in Figure 1. Bearing in mind the hydrometeor profiles illustrated in Figures 1b and 1d, we can appreciate the emission and the scattering contributions due to the prevailing presence of certain hydrometeors at various altitudes. In general, ice particles (graupel and ice crystals and aggregates) give a strong contribution of scattering which is greater at 85

GHz than at 19 GHz. Therefore this effect is particularly noted in cumulonimbi where scattering contributions at 85 GHz come from middle-height layers of the cloud. Vice versa, emission contributions are mainly due to raindrops and cloud droplets and are more significant at 19 GHz than at 85 GHz, where a sort of shadowing effect of the layers at lower altitudes is observed [*Smith et al.*, 1992]. For stratiform clouds, the multiple scattering is much smaller than the emission contribution and also smaller with respect to that of cumuliform clouds.

Scattering and emission effects have an indirect consequence on the value of brightness temperatures observed from the satellite. In general, scattering effects tend to lower T_B because of the presence of a cold sky, while emission effects tend to increase T_B. However, these tendencies are the result of interaction with the surface underneath, which acts as a direct source of radiation, but it also diffuses the radiation downwelling from the atmosphere. These influences are illustrated in Figures 4 and 5 where scatterplots of brightness temperatures are shown for pairs of frequencies and for various cloud genera over land and for summer conditions. Figure 6 shows the same but for different surface background and meteorological conditions (the results are shown only for cumulonimbi, cumuli congesti, altocumuli, and cirri). As a reference, in the previous figures the mean values of the upwelling T_B in clear-air conditions over land and over sea for both summer and winter cases are also shown. Finally, Figure 7 shows the histograms of simulated T_B at 19 and 85 GHz over land and over sea for cumulonimbi, cumuli congesti, nimbostrati, and strati.

As expected, cloud genera where liquid water content is predominant and without precipitating ice (like stratus and altocumulus) tend to raise T_B values with respect to clear-air ones. On the contrary, clouds producing appreciable precipitation (like nimbostratus, cumulus congestus, and cumulonimbus) yield a strong depression of T_B values at 85 and 37 GHz and a moderate decreasing at 19 GHz with respect to clear-air values. Cloud genera like altostrati and cirri behave in an intermediate way; in particular, the cirrus T_B exhibit small variations around the clear-air values due to the complete ice nature of this cloud genus.

It is noted that in the case of land surface, because of the higher radiation it produces, the emission effects due to liquid water particles become less evident compared with the sea surface case. There is also a significantly smaller dynamic range for altostrati, altocumuli, and cirri, that is, optically thin clouds, with respect to cumulonimbi, cumuli congesti, and nimbostrati. Note from Figure 6 that the effect of winter meteorological conditions is to cause a smaller dispersion of cloud points in the T_B planes.

4. Automatic Classification of Cloud Genera

The simulated database of genus cloud structures and brightness temperatures allows us to design a supervised automatic classifier. In order to make a simulated independent test the whole database consisting of 4500 realizations has been subdivided into a training set and a test set. The training set consists of 2250 points, corresponding to half the points of the whole database randomly selected within each cloud genus; the remaining points (2250) have been attributed to the test set.

As already mentioned, the random parameters of the database are the hydrometeor contents within each layer, the cloud levels, and the embedded meteorological profiles. The surface emissivity, described by the models illustrated in the previous section, has not been assumed to be random for this application. Of course, this choice has to be remembered when dealing with satellite measurements since it can produce a degradation of the estimate accuracy. We have generated eight brightness temperature databases, that is, over land and over sea for spring, summer, autumn, and winter meteorological conditions. In general, for the classification we have considered only the T_B frequencies at 19, 37, and 85 GHz. Thus, over land, the brightness temperature vector $\mathbf{T}_B$ has three components corresponding to the unpolarized T_B at each frequency. However, over the sea we have considered both the vertical (V) and horizontal (H) polarizations at each frequency by assuming a polarized specular emissivity for the sea. This means that over the sea the vector $\mathbf{T}_B$ has six components corresponding to 19, 37, and 85 GHz for both V and H channels, thus enhancing the discrimination capability of the cloud genera classifier.

The maximum likelihood (ML) criterion consists of maximizing the multivariate probability of the brightness temperature vector conditioned to the considered class [*Richards*, 1986]. We have assumed a multivariate Gaussian distribution for the brightness temperature vector so that to specify the discriminant function only the mean vector (centroid) and covariance matrix are needed. Actually, RTE describes a nonlinear process so that the T_B distribution turns out to be not necessarily Gaussian. However, two reasonings must be considered:

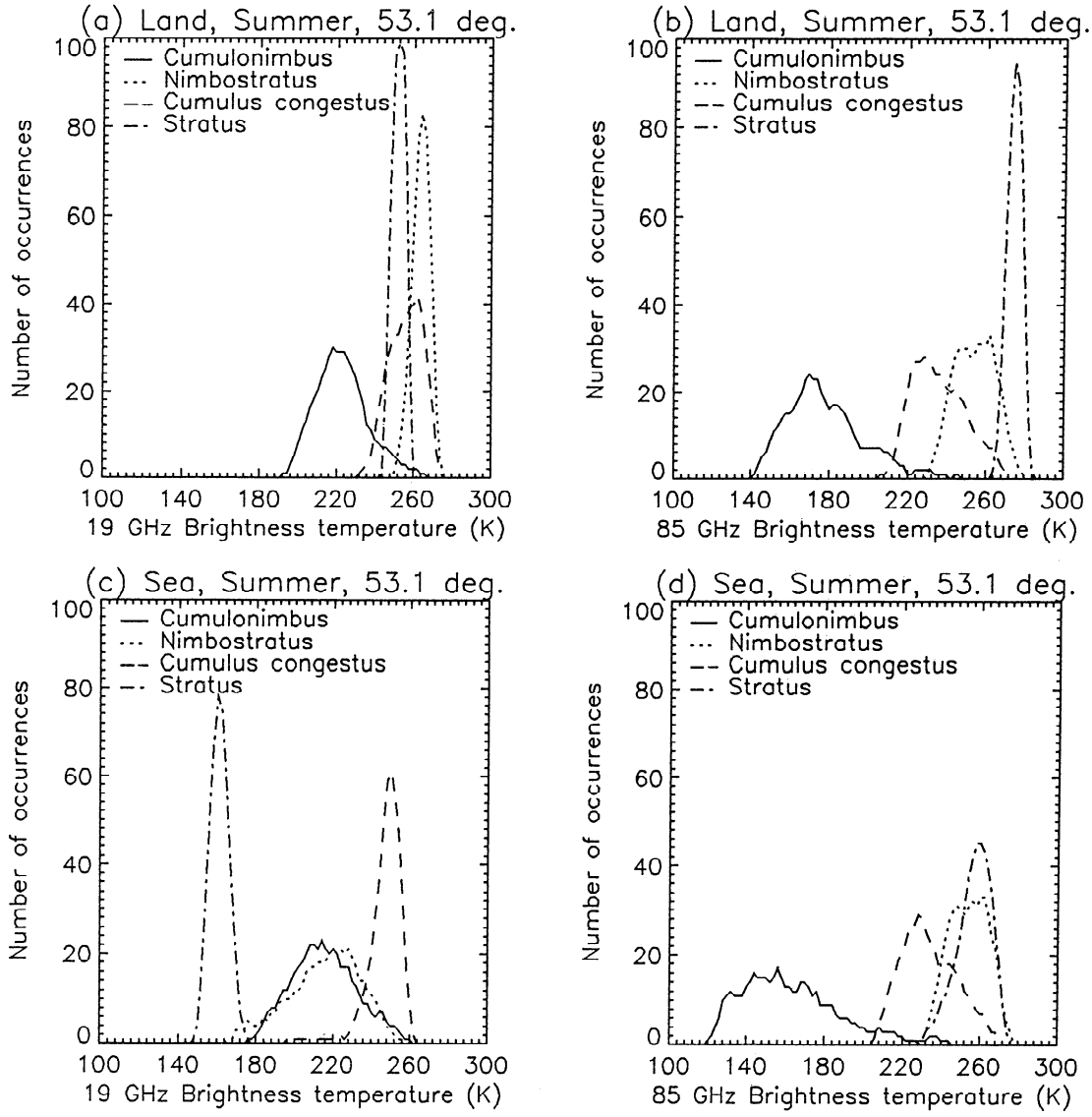

Figure 7. Histograms of simulated 19-GHz T_B (Figures 7a and 7c) and 85-GHz T_B (Figures 7b and 7d) for cumulonimbus, nimbostratus, cumulus congestus and stratus observed at 53.1° off-nadir angle during summer over land (Figures 7a and 7b) and over the sea (Figures 7c and 7d).

(1) We have restricted the analysis to each cloud genus so that the range of variation of the cloud parameters is limited, thus reducing the nonlinearity (like a stepwise regression); this is one of the advantages of the classification procedure. (2) By analyzing the marginal probability density functions (pdf's) of T_B of each cloud genus (e.g., Figure 7), the results is that most cloud genera have a Gaussian-like distribution, having only cumulonimbi a slight skewness due to some presence of congestus-like structures (although, as is known, the Gaussian form of the marginal pdf is not sufficient proof when dealing with multivariate pdf's). Analytically, the ML criterion implies the minimization of the following discriminant function d:

$$d(\mathbf{T}_{B\text{meas}}, i) = (\mathbf{T}_{B\text{meas}} - \mathbf{T}_{B\text{avg}i})^T \mathbf{C}_{TBi} (\mathbf{T}_{B\text{meas}} - \mathbf{T}_{B\text{avg}i}) + \ln[\det(\mathbf{C}_{TBi})] - \ln(P(i)) \quad (5)$$

where $\mathbf{T}_{B\text{meas}}$ is the measurement vector, $\mathbf{T}_{B\text{avg}i}$ and $\mathbf{C}_{TBi}$ are the mean vector and the covariance matrix of ith

Table 2. Confusion Matrix for Maximum-Likelihood Classification Over Land During Summer, Obtained From the Simulated Test Using 19-, 37-, and 85- GHz Unpolarized T_B

	Cu med	Cu con	Cb	Cb incus	St	Ns	As	Ac	Ci
Cu med	58.8	0	0	0.8	21.2	1.6	17.2	0.8	0.8
Cu con	0	73.2	5.2	0	0	8	0	0	0
Cb	0	2.4	88	12.4	0	0	0	0	0
Cb incus	0	0.8	6	70	0	0.8	0	0	0
St	23.6	0	0	0	48	0	12	15.6	0
Ns	0	21.2	0.8	12	0.4	84.4	0.8	0	0
As	4	2.4	0	4.8	1.2	5.2	68.8	0	0
Ac	10	0	0	0	26.4	0	1.2	68.8	6.8
Ci	3.6	0	0	0	2.8	0	0	14.8	92.4

class, respectively, $\det(\mathbf{C}_{TBi})$ is the determinant of $\mathbf{C}_{TBi}$, i is the ith cloud genus, and $P(i)$ is the a priori probability of the ith class. The latter probability may be useful to impose a priori information about the cloud scenario to the automatic classifier, but in this work we have set it as uniform. Both $\mathbf{T}_{Bavgi}$ and $\mathbf{C}_{TBi}$ have been computed from each seasonal simulated database relative to each modeled cloud genus.

Tests have been performed by adding to the T_B test set a Gaussian error with 1-K standard deviation and zero mean. In order to analyze the results we have introduced the so-called confusion matrix, which gives the percentage probability of identification of a certain cloud genus. Table 2 shows the confusion matrix for SSM/I simulations over land during summer, while Table 3 shows the same but for simulations over the sea using polarized T_B as a measurement vector. Note that columns represent true cloud genera and rows represent the classified ones being 100% the sum of the percentages along each column. The diagonal terms of the confusion matrix indicate the percentage of right classification, while the off-diagonal terms refer to the percentage of misclassified cases. From the confusion matrix itself, it is possible to derive the total mean error as the average of the classification errors which are obtained for each class by summing the off-diagonal percentages along the column.

The first evidence is that the total mean error is much lower over the sea (about 17%) than over land (about 27%). This result was expected, since, on one hand, over the sea optically thin clouds are much more separated in terms of radiometric signature (see Figure 7) and, on the other hand, over the sea the measurement vector has a dimension which is double with respect to the land case. Both over land and sea the cumuliform clouds are well classified, with errors less than 25% over land and less than 15% over the sea, even though the classifier often confuses cumuli congesti for nimbostrati. The larger misclassification errors are made on stratus clouds,

Table 3. Same as for Table 2, But Over the Sea and Using 19-, 37-, and 85-GHz Vertical and Horizontal Polarized T_B

	Cu med	Cu con	Cb	Cb incus	St	Ns	As	Ac	Ci
Cu med	70.4	0	0	0	7.6	2	5.2	0	0
Cu con	0	83.6	5.6	0	0	7.2	0	0	0
Cb	0	5.2	92.8	18.4	0	0	0	0	0
Cb incus	0	0	1.2	74	0	0	0	0	0
St	16.8	0	0	0	66.4	0	15.6	3.6	0
Ns	1.2	10.8	0.4	6	0	88.4	1.2	0	0
As	5.6	0.4	0	1.6	5.6	2.4	78	0	0
Ac	6	0	0	0	19.6	0	0	94	0.8
Ci	0	0	0	0	0.8	0	0	2.4	99.2

which are frequently confused with altocumuli and cumuli mediocres.

As a comparison, we have also applied to the database an automatic classifier based on a neural network. We have chosen a supervised feed-forward network with a Kohonen learning rule [*Kohonen*, 1987]. Apart from the input neurons (or layer), the network consists of a hidden competitive layer plus a linear output layer. The number of neurons of the hidden layer has been set to 36, while the number of learning cycles has ranged from 20,000 up to 30,000, with a learning rate of 0.01. Using the above configuration, the total mean error has been 23% over land and 19% over the sea thus showing better results over land but slightly worse results over the sea when compared with the ML algorithm. In a certain sense the similar performances of the two classification methods may indicate that the assumption of a Gaussian distribution of T_B within each cloud genus is fairly acceptable. Even though the neural network represents a promising tool for implementing an automatic classifier [*Lee et al.*, 1990], in this work we have finally adopted the maximum likelihood classifier.

5. Tests on SSM/I Data

Although an exhaustive validation of the simulation results is not within the scope of this work, we have tested the produced genus database in different ways. Often the comparisons have been made using SSM/I data on a statistical basis, but where possible we have taken note of the corresponding meteorological conditions and their evolution and of data gathered from other sensors. Objective difficulties arise when a direct comparison with the cloud truth is attempted, and information taken from other sensors cannot always solve the ambiguities.

In the case of precipitating clouds, rain gauge networks can give sparse information on the time-averaged surface rain rate due to the cloud system, but this is not always consistent with spatially averaged instantaneous estimates derived from satellite radiometers. Ground-based meteorological radars can provide rain rate maps even though there is generally a minimum altitude (of the order of hundreds of meters above the surface) below which the ground clutter becomes predominant [*Bogush*, 1989]. Satellite IR and VIS radiometers can give only rough estimates of rainfall rate and cloud characteristics [*Marroccu et al.*, 1993].

In the case of nonprecipitating clouds, subjective visual evaluations carried out by following the Cloud Atlas instructions can be made but with an accuracy not easy to determine quantitatively. Combination of IR and VIS channels of satellite radiometers can provide statistical features useful to classify images in terms of cloud genera and properties [*Garand*, 1988]. The way in which VIS-IR radiometers probe cloud systems can furnish information about the cloud top altitude and morphology but does not yield cloud vertical characteristics.

In this section we report various tests using the SSM/I data. We have tried both a statistical intercomparison of SSM/I measurements with cloud database radiometric simulations and the analysis of a case study where SSM/I, ground-based radar, and Meteosat were almost contemporaneously available. The SSM/I data have been selected by considering those cases where there is either a large set of ground-based observations or a well-detailed description of meteorological validations.

5.1. Statistical Analysis

Figure 8 shows the comparison between the histograms of simulated T_B at 19 and 85 GHz looking at 53.1° off-nadir for nimbostrati, cumuli congesti, and cumulonimbi over land with those derived from SSM/I images relative to three flood cases which occurred in Italy in the last decade. We will refer to them as the Arno, Valtellina, and Liguria cases. Table 4 shows the results of the cloud genus classification in terms of the number of occurrences obtained by applying the ML classifier to each analyzed case.

A previous discrimination of precipitation areas was performed by applying the scattering index (SI) algorithm described by *Ferraro et al.* [1994] so that only pixels containing precipitating clouds have been selected. This is the reason why we report in the figure only simulated cloud genera with RR>3 mm/hr. Note that the histograms are shown in terms of number of occurrences, and SSM/I T_B at 19, 22, and 37 GHz have been deconvolved to the ground resolution of 85-GHz T_B (about 15 km) by means of a Backus-Gilbert filtering [*Farrar and Smith*, 1992].

In all the three cases, cold front passages are involved. During the passage of a cold front the abrupt lifting of warm air caused by the front itself produces cumulonimbus formation in the very passage accompanied with nimbostrati and cumuli ahead and behind the front. Therefore the genera of clouds we observed from SSM/I data are dependent on the time of the satellite overpass with respect to the passage of the cold front.

The first case (Figures 8a and 8b) refers to the Arno River (Italy) event. It has been described and analyzed by *Pierdicca et al.* [1996] and refers to a winter frontal

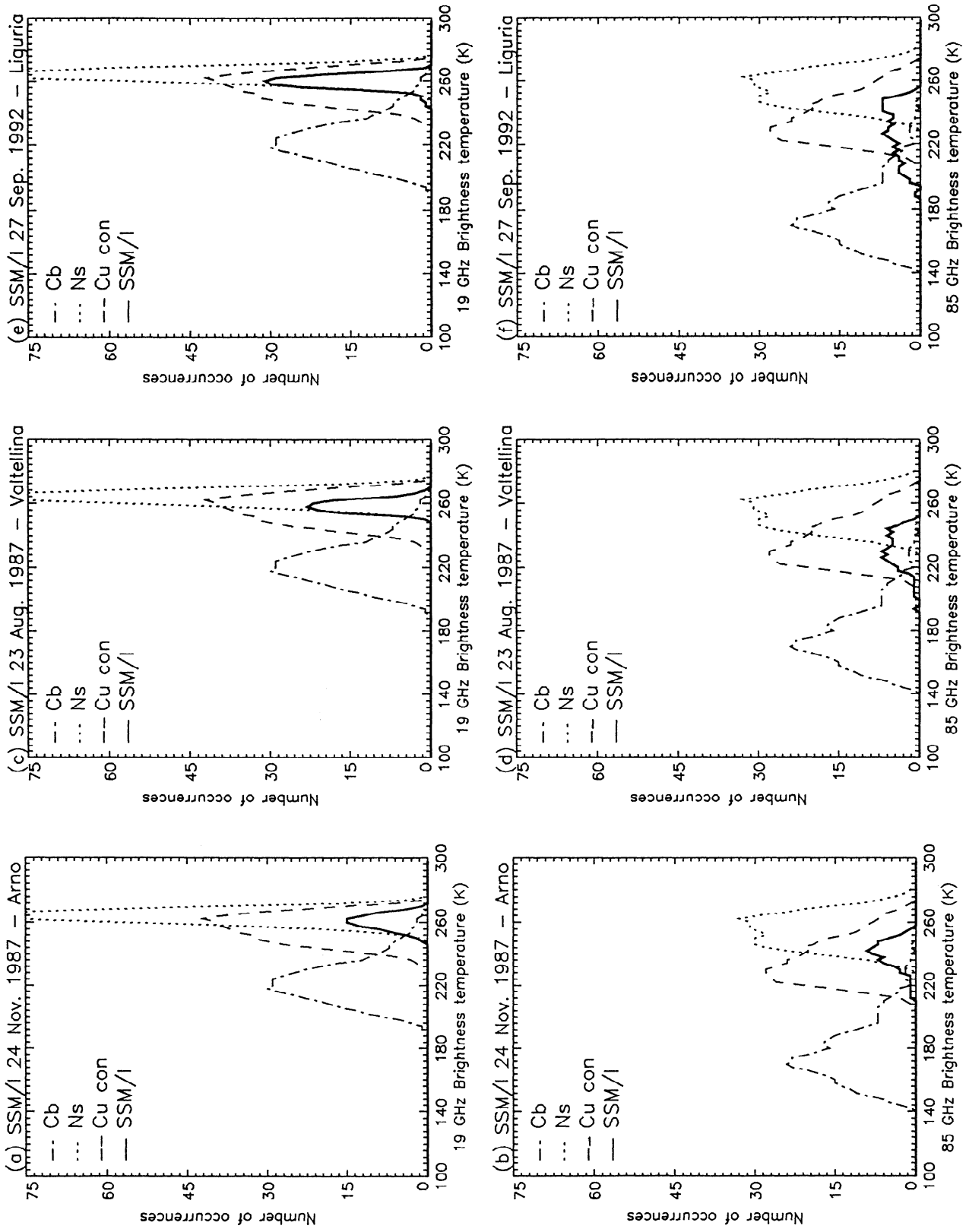
(a) SSM/I 24 Nov. 1987 – Arno
(b) SSM/I 24 Nov. 1987 – Arno
(c) SSM/I 23 Aug. 1987 – Valtellina
(d) SSM/I 23 Aug. 1987 – Valtellina
(e) SSM/I 27 Sep. 1992 – Liguria
(f) SSM/I 27 Sep. 1992 – Liguria
Cb
Ns
Cu con
SSM/I
Number of occurrences
19 GHz Brightness temperature (K)
85 GHz Brightness temperature (K)

Table 4. Number of Cloud Genera Derived From the Application of the Maximum-Likelihood Classifier to Six Cases

	Cu med	Cu con	Cb	Cb incus	St	Ns	As	Ac	Ci
Arno case	0	14	0	0	0	84	0	0	0
Valtellina case	0	14	1	14	0	92	0	0	0
Liguria case	0	49	2	21	0	99	0	0	0
Milan site	1	25	0	1	0	136	7	0	9
AIP-2 case front region	114	97	0	0	5	728	60	5	0
AIP-2 case entire image	561	509	0	0	95	2740	194	170	1

AIP-2, Algorithm Intercomparison Project 2.

system imaged by SSM/I on November 24, 1987, at 1800 UTC when it had already passed through Tuscany, leaving rainy stratiform clouds with relatively low rainfall rates (the intense precipitation occurred before, on November 23). From histogram comparison and from Table 4 it emerges that nimbostrati were predominant within the Arno basin, together with a small number of cumuli congesti. Moreover, note that the simulated database of nimbostrati gives rain rates less than 15 mm/hr which are in fairly good agreement with surface RR measured by the rain gauge network of the Arno basin during this event.

The second case (Figures 8c and 8d) refers to the Valtellina valley (Italy) event of August 23, 1987, which has been analyzed in detail by *Levizzani et al.* [1996]. The heavy and long-lasting precipitation was caused by a cold front approaching from northwest Atlantic regions. After passing through the southeast portion of France, the front reached the warm air coming from the Mediterranean lifted against the Alps, causing a series of storms along the front. Most of the clouds were of both cumuliform and stratiform type with surface rain rates up to 20 mm/hr during the overpass of SSM/I on August 23, 1987, at 1821 UTC, which did not catch the actual passage of the cold front. This analysis can be compared with information derived from T_B histograms at 19 and 85 GHz and from Table 4. The result is that the most probable cloud genus was the nimbostratus with a relatively small presence of cumuli congesti and cumulonimbi. A comparison (not shown) between the histograms of rain gauge RR and SSM/I-derived RR shows fairly good agreement for both the mean and the variance of rain rate values.

The third case is relative to the Liguria (Italy) flash flood which happened on September 27, 1992, and whose images were acquired by SSM/I at 1555 UTC [*Levizzani et al.*, 1996]. A frontal system was able to travel toward Italy from the southwest that originated by the merging of two depressions over Spain and North Africa. The fast front approached a warm and humid surface air current coming from the southern Mediterranean around 1200 UTC. Violent prefrontal storms developed along the Liguria coasts in the early afternoon. The storm system was characterized by convective cells with a strong vertical development and a high surface rainfall rate with measured rain gauge values up to 50 mm/hr. It is interesting to note that the histogram of measured T_B at 85 GHz is much more spread with respect to the other cases and that a relevant number of cumulonimbi T_B are covered by SSM/I measurements. The T_B histogram and Table 4 also indicate a considerable presence of nimbostrati with cumuli congesti and cumulonimbi.

Figures 9a and 9b show the scatterplots of SSM/I

Figure 8. Histograms of simulated (left) 19-GHz T_B and (right) 85 GHz T_B over land for rainy cloud genera (Ns, Cu con and Ns) observed at 53.1° off-nadir angle as compared to special sensor microwave imager (SSM/I) measurements during the Arno River case on November 24, 1987, (Figures 8a and 8b), the Valtellina valley case on August 23, 1987, (Figures 8c and 8d) and the Liguria case on September 27, 1987, (Figures 8e and 8f).

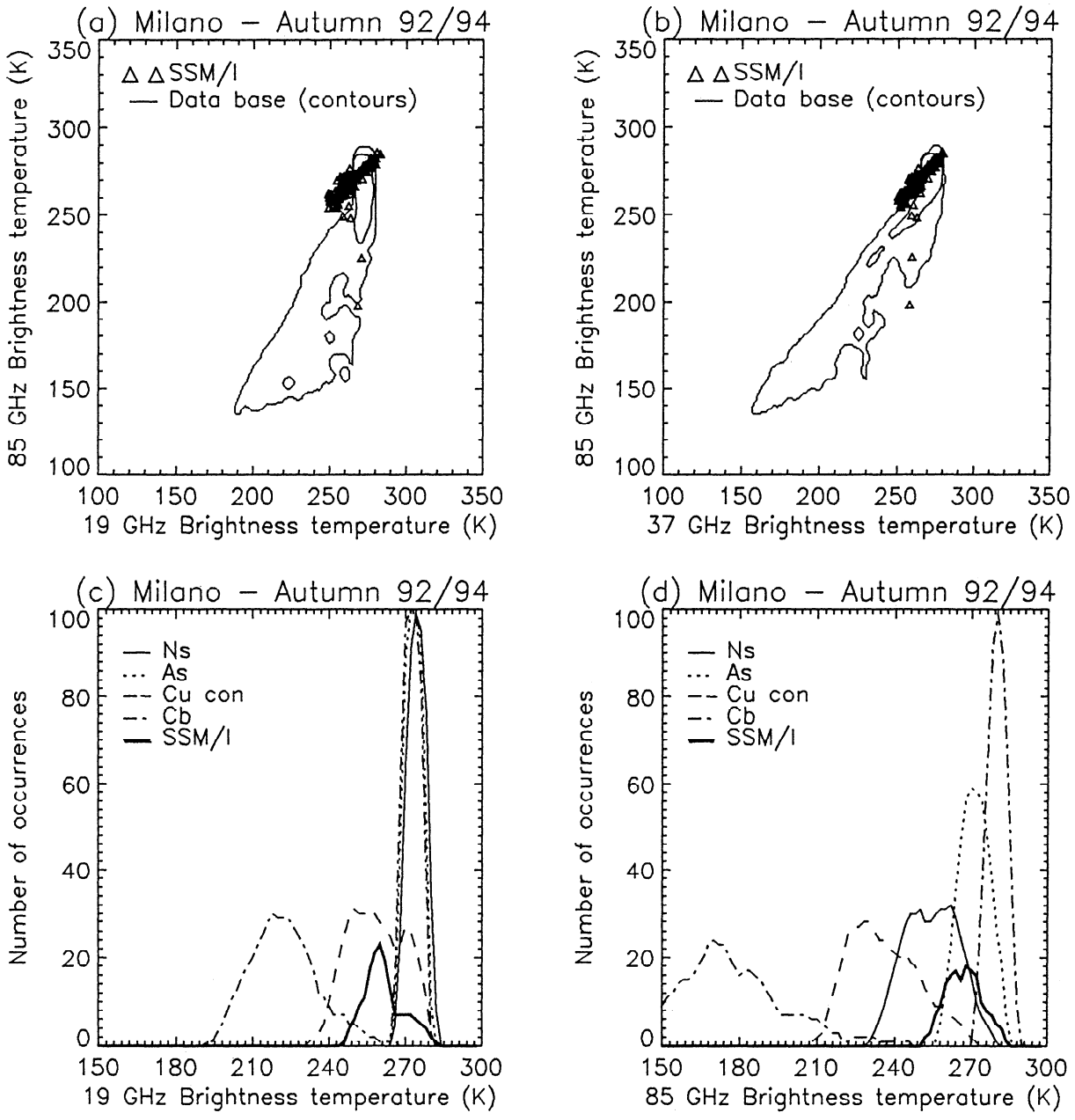

Figure 9. Scatterplots of SSM/I measurements (average of V and H polarizations) at (a) 19 and 85 GHz and (b) at 37 and 85 GHz, acquired over Milan, Italy, at 45.4° N, 9.5° E during the autumnal period of 1992 and 1994, superimposed over the whole modeled database (indicated on the T_B plane by contour lines of the point density histogram with a step of 350 and a bin of 5 K). Histograms of simulated (c) 19-GHz T_B and (d) 85-GHz T_B observed at 53.1° off-nadir angle over land during autumn for altostrati, nimbostrati, cumuli congesti, and cumulonimbi as compared to SSM/I measurements over Milan.

measurements for selected pairs of frequencies, acquired over Milan, Italy, at 45.4° N, 9.5° E during the autumnal period of 1992 and 1994 and superimposed over the whole modeled T_B database (indicated on the T_B plane by contour lines of the point density histogram). Figures 9c and 9d show the histograms of simulated 19-GHz T_B and 85-GHz T_B, respectively, observed at 53.1° off-nadir angle over land during autumn for altostrati, nimbostrati,

cumuli congesti, and cumulonimbi as compared again with SSM/I measurements over Milan. It is worth noting that in this case we did not select the SSM/I measurements to discriminate precipitation, so that measured T_B refers to various meteorological conditions in that area during autumn. Mean meteorological profiles have been adapted to the season and location under analysis. The clear-air T_B over land are 269.5, 270.2, and 277.9 K at 19, 37, and 85 GHz, respectively. Note that SSM/I lower channel T_B have not been deconvolved and that this causes a stronger impact of beam filling errors due to horizontally finite clouds.

Figures 9a and 9b indicate a fairly good adequateness of the modeled database at 37 and 85 GHz to represent the SSM/I measurement variability. The slight discrepancy observed at 19 GHz is possibly due to the variability of surface background (not taken into account in this simulation) and to inhomogeneities within the larger field of view at 19 GHz (about 60 km) with respect to the other SSM/I frequencies.

It is interesting to remark that from a climatological point of view, during autumn in the Po valley where Milan is situated, there is a scarcity of thunderstorm activity with a prevalence of stratiform clouds due to perturbations coming from the western Mediterranean and the northern Atlantic Ocean (cumuliform clouds, characterized by intense and short rainfalls, are basically typical of springtime and the warmest periods of summer). The mean number of rainy days in Milan during autumn is around 40, with cumulative precipitation ranging from 200 to 300 mm. Indeed, from the histograms of Figures 9c and 9d and Table 4, it appears that cumulonimbi are not detected, while low (strati and nimbostrati) and middle-high (altocumuli and cirri) clouds are present with some cumuli congesti.

5.2. Case Study

During the Algorithm Intercomparison Project 2 (AIP-2), multisensor observations of an area covering central western Europe have been made available to research groups [*Allam et al.*, 1993]. In particular, the data set mainly consisted of SSM/I and Meteosat data acquired during February and March 1991 together with RR maps derived from a ground-based radar network.

Figure 10 shows the images of SSM/I data at 19 and 85 GHz (average of V and H polarizations) on February 21, 1991, at 0837 UTC during the AIP-2 campaign. The SSM/I images are shown in the sensor coordinates so that deformations of coastal lines are apparent. A frontal system over ocean originating from the Atlantic Ocean is detectable from the images which show a fairly strong radiometric signature starting from southern England and covering the bay of Biscay and partially the Brittany peninsula (France); note that we will not comment on the cloudy area over the North Sea. Widespread storms were produced when the front approached the Atlantic coasts. Within the front the T_B values at 85 GHz are greater than 200 K, while T_B at 19 GHz are less than 190 K; these T_B values should anticipate that the presence of cumulonimbi is negligible in that area (see Figures 7c and 7d).

The SSM/I images can be compared with AIP-2 available measurements. Figure 11 shows the Meteosat image at IR band acquired on February 21, 1991, at 0900 UTC together with the rainfall rate map derived from radar network during the AIP-2 campaign [*Allam et al.*, 1993], both projected in polar stereographic coordinates. The white areas in the IR image are associated with colder temperatures, thus denoting high cloud top altitudes. Black zones indicate surface background, either ocean or land, while gray scale regions denote cloudy systems. The radar RR map shows values less than 16 mm/hr with precipitation coverage mainly over ocean.

In order to apply the ML automatic classifier, we need to discriminate the cloud coverage area within the SSM/I images. Since references in literature concern only discrimination of precipitation area (e.g., see *Ferraro et al.*, 1994), we have developed a tree algorithm characterized by thresholds on both polarized T_B and scattering index. In particular, the algorithm we have applied to each image pixel provides the masks of clouds both over land and over the sea. Defining the vertical and horizontal polarization averages at 19 and 85 GHz as TB19U=0.5 $[T_B(19V)+T_B(19H)]$ and TB85U=0.5 $[T_B(85V)+T_B(85H)]$, respectively, and the polarization difference at 19 GHz as ΔTB19= $T_B(19V)$-$T_B(19H)$, the algorithm can be schematically formulated as follows:

1. If TB19U<210 K and ΔTB19>35 K, then the pixel refers to sea background. In case of sea background, by applying the definition of the scattering index over water (SIW) [*Ferraro et al.*, 1994], if SIW>10 K, then a convective cloud is present, else if TB85U>235 K, then the pixel possibly refers to a stratiform cloud. After cloud presence detection, the ML algorithm is applied using the cloud databases for sea surface.

2. If TB19U>230 K and ΔTB19<30 K, then the pixel refers to land background; note that if neither land nor sea conditions are met, the pixel refers to coast background. In case of land background, by applying the

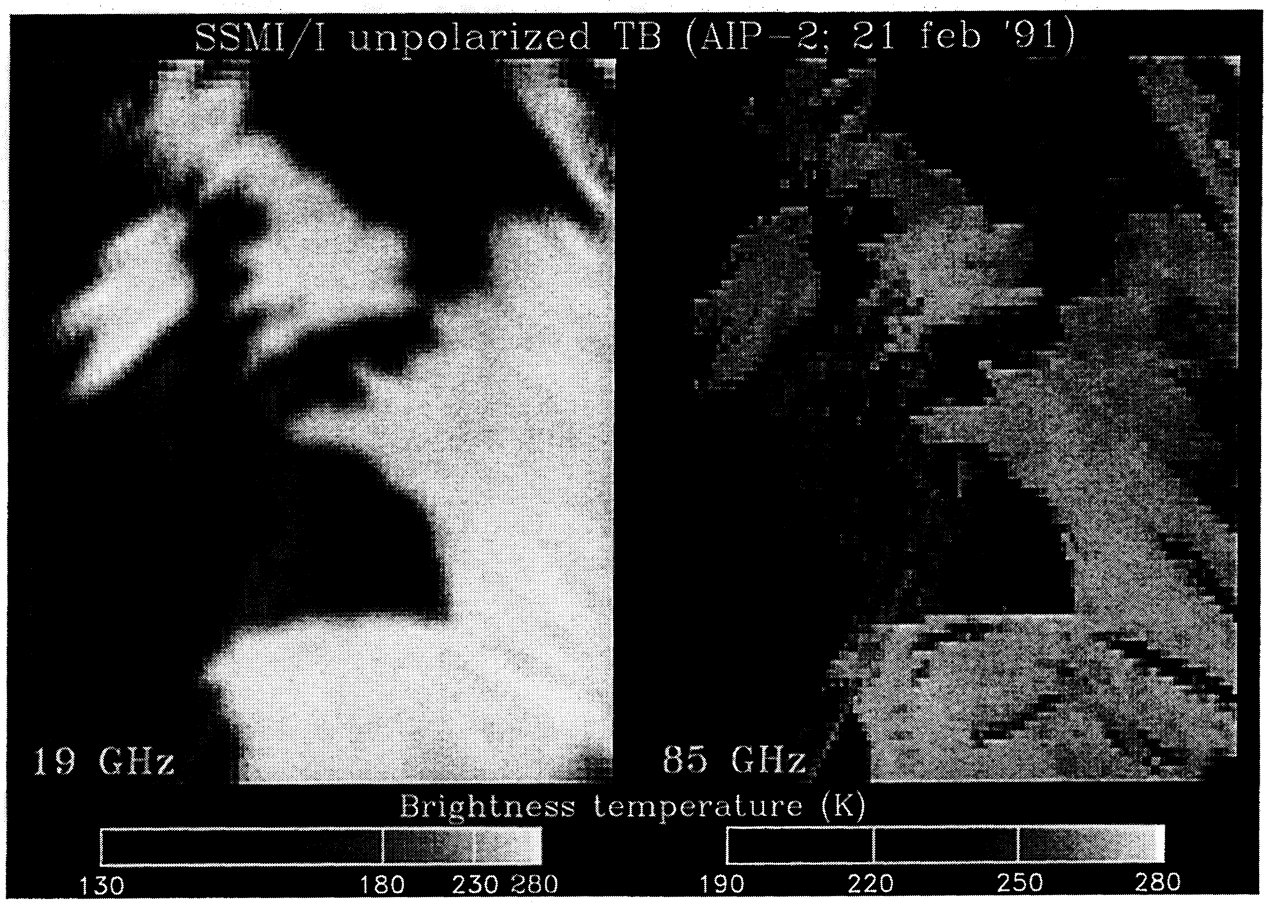

Figure 10. Images of SSM/I data at 19 and 85 GHz (average of V and H polarizations) on February 21, 1991, at 0837 UTC during Algorithm Intercomparison Project 2 campaign.

definition of the scattering index over land (SIL) [*Ferraro et al.*, 1994], if SIL>5 K and $T_B(22V)> 264$ and $T_B(22V)>[175+0.49\ T_B(85V)]$ is satisfied, then the pixel refers to cloud over land and the ML algorithm is applied using the cloud databases for land surface; otherwise it is snow coverage.

Note that the above algorithm has been also tested on other AIP-2 cases but not systematically validated on a large set of SSM/I cases in different climatic regions and conditions.

Figure 12 shows a cloud genus map derived from SSM/I data acquired on February 21,1991, at 0837 UTC by applying the ML classification algorithm. The gray-scale palette and Table 4 (front region) indicate that most of the clouds in the front region are nimbostrati with some presence of either cumuli mediocres or cumuli congesti. These results are quite consistent with IR temperature image shown in Figure 11, even though the low-altitude cloud coverage over Brittany and along the Atlantic French coast is not properly detected. This can be explained by noting that the discrimination of optically thin clouds over land from SSM/I data is impaired by the poor contrast between cloud and land T_B signature; on the contrary, the case of convective clouds over land can be easily addressed since the large scattering contribution can give strong depressions of 85-GHz T_B with respect to clear-air T_B values over land.

Figure 13 shows the rainfall rate map derived from SSM/I data by applying the maximum a posteriori probability (MAP) estimation method [*Pierdicca et al.*, 1996] for each cloud genus, previously identified. This implies that for each pixel we have used as a training data set the database of the specific cloud genus. In other words, the cloud classification procedure can be seen as the first step of a precipitation retrieval algorithm. The coverage of estimated rain rate map is fairly

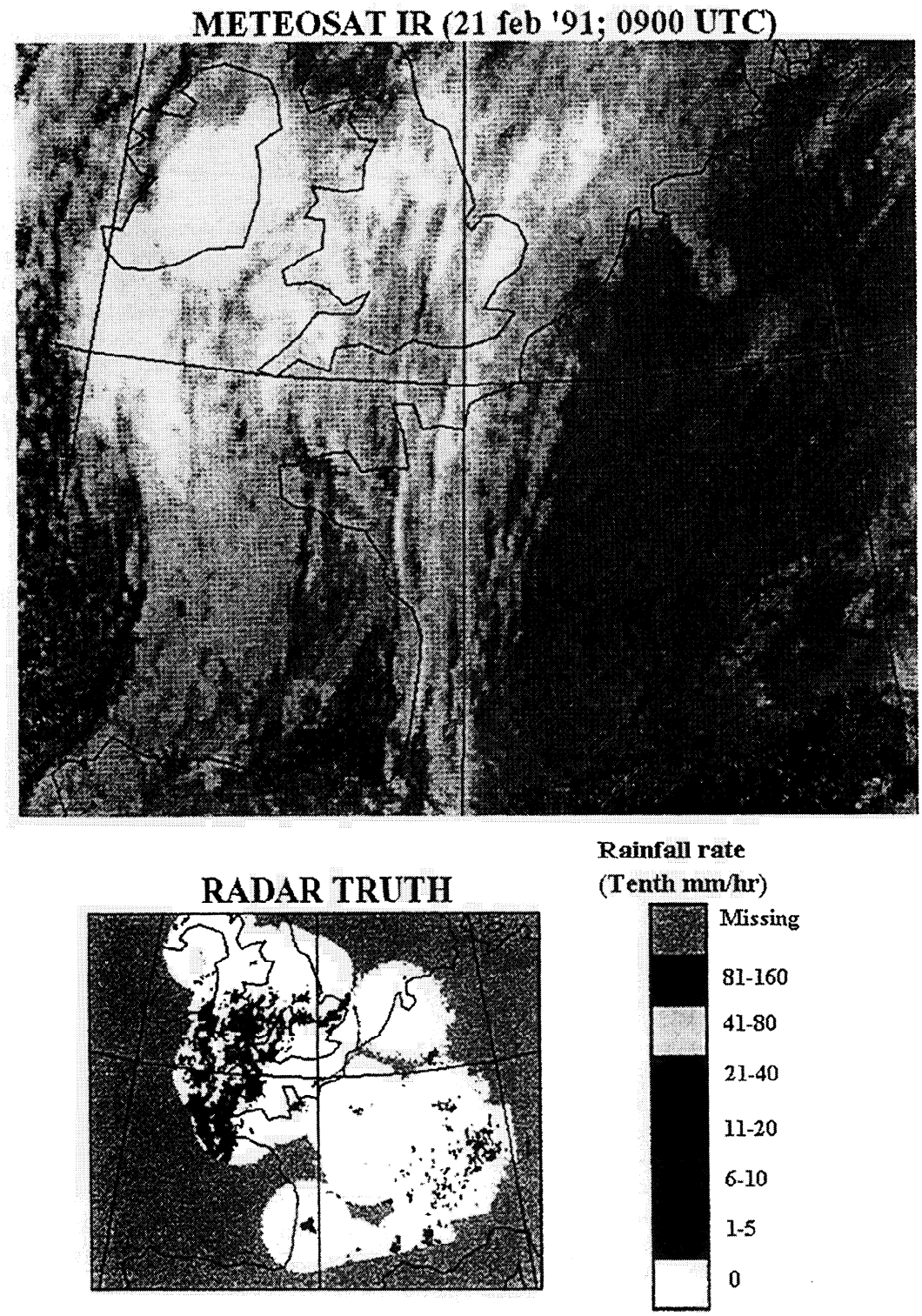

Figure 11. Meteosat image at IR band acquired on February 21, 1991, at 0900 UTC, together with rainfall rate map derived from radar network during AIP-2 campaign [after *Allam et al.*, 1993].

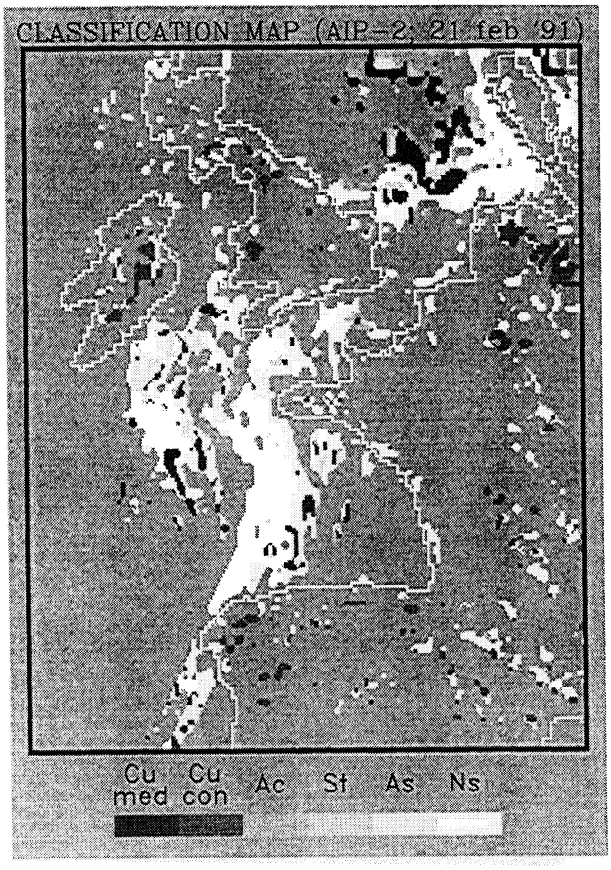

Figure 12. Cloud genera map derived from SSM/I data acquired on February 21, 1991, at 0837 UTC by applying the maximum-likelihood (ML) classification algorithm after discriminating the cloud coverage, as explained in the text.

similar to that derived from the radar (see Figure 11), and the range and pattern of estimated RR are also in fairly good agreement with the radar ones.

6. Conclusions

In this work we have established a database of hydrometeor profiles of clouds and of the corresponding simulated brightness temperatures, for each type of cloud, defined according to a classification based on genera and species. In this way we remain within the framework of a classification which is widely studied and recognized by the meteorological scientific community. Without attempting a thorough validation of the results, for which a large set of data gathered with different sensors and over a long time would be required, we have tested several specific cases by using meteorological information, radar, and rain gauge data. Tests are mainly carried out examining and analyzing SSM/I images of several months and various locations. Two testing paths have been followed. In some cases, where meteorological conditions in a given area were quite well known and assessed, the SSM/I brightness temperatures relative to that area are reported in the simulated brightness temperature scatterplots and histograms for comparison, and an image analysis is also made. In other cases, brightness temperatures relative to specific locations are examined all together, giving a climatological outline of the locations themselves.

However, some unsolved or puzzling problems have arisen during the analysis of SSM/I images, and indeed these are intrinsic to any kind of cloud classification.

1. Seldom is there a sole genus of cloud present within the same area (i.e., image pixel). Consider what is happening when a weather front is approaching and often several genera of clouds are present simultaneously.

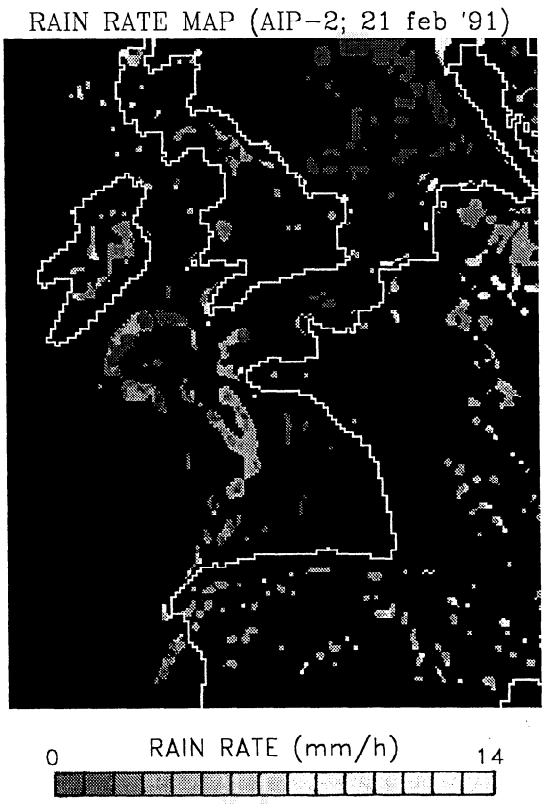

Figure 13. Rainfall rate maps estimated from SSM/I data acquired on February 21, 1991, at 0837 UTC by using the maximum a posteriori probability estimation method after applying the ML cloud classifier.

In such cases a superclassification based on high, middle, and low clouds may be needed, and meteorology can help in defining possible cloud stratifications.

2. Many genera of clouds are horizontally limited, at least within the field of view of the radiometer. A filling factor could be estimated, but the effects of the surface background become important and must be taken into account.

3. Surface emissivity can play a significant role when classifying cloud genera which are optically thin and present a lower amount of ice, like stratiform and cirriform clouds. A choice could be to adopt more sophisticated models of surface emissivity and let the emissivity itself vary randomly within given limits (possibly experimentally derived).

4. Microwave radiometers have a different horizontal resolution in the various channels. A deconvolution or averaging process is therefore needed.

Acknowledgments. This work has been partially supported by the Italian Space Agency (ASI) and the Ministry of University and Research (MURST). The SSM/I data have been provided by the Distributed Automatic Archive Center (DAAC) of NASA's Marshall Space Flight Center (MSFC), while AIP-2 data have been furnished by the U.K. Meteorological Office. The brightness temperature databases of each modeled cloud genus (or the mean vectors and covariance matrices of the automatic cloud classifier) are available to research groups on request.

References

Allam, R., G. Holpin, P. Jackson, and G.L. Liberti, Second Algorithm Intercomparison Project of the Global Precipitation Climatology Project: AIP-2, preworkshop report, 133 pp., U.K. Meteorol. Off., Bracknell, England, 1993.

Basili, P., P. Ciotti, G. d'Auria, F.S. Marzano, and N. Pierdicca, A microwave radiometry characterization of precipitating clouds, in *Microwave Radiometry and Remote Sensing Applications*, edited by D. Solimini, pp. 229-249, VSP, Utrecht, Netherlands, 1995.

Bogush, A.J., *Radar and the Atmosphere*, Artech House, Norwood, Mass., 1989.

Bohren, C.F., and D.R. Huffman, *Absorption and Scattering of Light by Small Particles*, John Wiley, New York, 1983.

Desbois, M., G. Seze, and G. Szejwach, Automatic classification of clouds on Meteosat imagery: Application to high level clouds, *J. Appl. Meteorol.*, *21*, 401-412, 1982.

Evans, K.F., J. Turk, T. Wong, and G. Stephens, A Bayesian approach to microwave precipitation profile retrieval, *J. Appl. Meteorol.*, *34*, 260-279, 1995.

Farrar, M.R., and E.A. Smith, Spatial resolution enhancement of terrestrial features using deconvolved SSM/I microwave brightness temperatures, *IEEE Trans. Geosci. Remote Sens.*, *30*, 349-355, 1992.

Ferraro, R.R., N.C. Grody, and G.F. Marks, Effects of surface conditions on rain identification using the DMSP-SSM/I, *Remote Sens. Rev.*, *11*, 195-209, 1994.

Garand, L., Automated recognition of oceanic cloud patterns, I, Methodology and application to cloud climatology, *J. Clim.*, *1*, 20-39, 1988.

Kohonen, T., *Self Organizing and Associative Memory*, 2nd ed., Springer-Verlag, New York, 1987.

Kummerow, C., On the accuracy of the Eddington approximation for radiative transfer in the microwave frequencies, *J. Geophys. Res.*, *98*, 2757-2765, 1993.

Kummerow, C., and L. Giglio, A passive microwave technique for estimating rainfall and vertical structure information from space, I, Algorithm description, *J. Appl. Meteorol.*, *33*, 3-18, 1994.

Kummerow, C., W.S. Olson, and L. Giglio, A simplified scheme for obtaining precipitation and vertical hydrometeor profiles from passive microwave sensors, *IEEE Trans. Geosci. Remote Sens.*, *34*, 1213-1232, 1996.

Lee, J, R.C. Weger, S.K. Sengupta, and R.M. Welch, A neural network approach to cloud classification, *IEEE Trans. Geosci. Remote Sens.*, *28*, 846-855, 1990.

Levizzani, V., F. Porcù, F.S. Marzano, A. Mugnai, E.A. Smith, and F. Prodi, Investigating a SSM/I microwave algorithm to calibrate Meteosat infrared instantaneous rain rate estimates, *Meteorol. Appl.*, *3*, 5-17, 1996.

Liebe, H.J., An updated model for millimeter propagation in moist air, *Radio Sci.*, *20*, 1069-1089, 1985.

Marroccu, M., A. Pompei, G. Dalu, G.L. Liberti, and A. Negri, Precipitation estimation over Sardinia from satellite infrared data, *Int. J. Remote Sens.*, *14*, 115-134, 1993.

Mugnai, A., and W.J. Wiscombe, Scattering of radiation by moderately nonspherical particles, *J. Atmos. Sci.*, *37*, 1291-1307, 1980.

Mugnai, A. and E.A. Smith, Radiative transfer through a precipitating cloud at multiple microwave frequencies, I, Model description, *J. Appl. Meteorol.*, *27*, 1055-1073, 1988.

Mugnai, A., E.A. Smith, and G.J. Tripoli, Foundations for statistical-physical precipitation retrieval from passive microwave satellite measurements, I, Emission source and generalized weighting function properties of a time dependent cloud-radiation model, *J. Appl. Meteorol.*, *32*, 17-39, 1993.

Pierdicca, N., F.S. Marzano, G. d'Auria, P. Basili, P. Ciotti, and A. Mugnai, Precipitation retrieval from spaceborne microwave radiometers using maximum a posteriori probability estimation, *IEEE Trans. Geosci. Remote Sens.*, *34*, 1-16, 1996.

Pruppacher, H.R., and J.D. Klett, *Microphysics of Clouds and Precipitation*, D. Reidel, Norwell, Mass., 1978.

Ray, P.S., Broadband complex refractive indices of ice and water, *Appl. Opt.*, *11*, 1863-1843, 1972.

Richards, J.A., *Remote Sensing Digital Image Analysis: An Introduction*, Springer-Verlag, New York, 1986.

Sekhon, R.S., and R.C. Srivastava, Snow size spectra and radar reflectivity, *J. Atmos. Sci.*, *27*, 299-307, 1970.

Smith, E.A., A. Mugnai, H.J. Cooper, G.J. Tripoli, and X. Xiang, Foundations for statistical-physical precipitation retrieval from passive microwave satellite measurements, I, Brightness temperature properties of a time dependent cloud-radiation model, *J. Appl. Meteorol.*, *31*, 506-531, 1992.

Stogryn, A., Equations for calculating the dielectric constant of saline water, *IEEE Trans. Microwave Theory Technol.*, *19*, 733-736, 1971.

Tripoli, G.J., A nonhydrostatic model designed to simulate scale interaction, *Mon. Weather Rev*, *117*, 1342-1359, 1992.

World Meteorological Organization, *Guide to Meteorological Instruments and Observing Pratices,* 4th ed., *WMO 8.TP.3*, Geneva, 1971.

Wu, R., and J.A. Weinman, Microwave radiances from precipitating clouds containing aspherical ice, combined phase, and liquid hydrometeors, *J. Geophys. Res.*, *89*, 7170-7178, 1984.

P. Basili, Istituto di Elettronica, Università di Perugia, Via G. Duranti, 93-06131 Perugia, Italy. (e-mail: basili@istel.ing.unipg.it)

P. Ciotti and F.S. Marzano, Dipartimento di Ingegneria Elettrica, Università di L'Aquila, Monteluco di Roio, 67040, L'Aquila, Italy. (e-mail: cpiero@dsiaq1.ing.univaq.it; franko@palatino1.ing.uniroma1.it)

G. d'Auria, R. Pinna Nossai, and N. Pierdicca, Dipartimento di Ingegneria Elettronica, Università "La Sapienza" di Roma, Via Eudossiana, 18-00184, Roma, Italy. (e-mail: gioda@palatino1.ing.uniroma1.it; roberto@aventino.ing.uniroma1.it; mauro@velia.ing.uniroma1.it)

(Received March 12, 1997; revised August 4, 1997; accepted August 28, 1997)